

Engine maps of fuel use and emissions from transient driving cycles



Justin D.K. Bishop^{a,*}, Marc E.J. Stettler^a, N. Molden^b, Adam M. Boies^a

^a Centre for Sustainable Road Freight, University of Cambridge, Department of Engineering, Trumpington Street, Cambridge CB2 1PZ, United Kingdom

^b Emissions Analytics, Manor Farm, Romsey Road, Pitt, Winchester, Hampshire SO22 5QX, United Kingdom

HIGHLIGHTS

- OBD ubiquitous in modern vehicles, PEMS to be regulatory requirement in Europe.
- Maps of transient fuel use, emissions recreated from real-world driving data.
- Trip-level fuel use and emissions within 5% of observed values generally.
- Per second fuel use and emissions simulated accurately.

ARTICLE INFO

Article history:

Received 26 November 2015

Received in revised form 8 August 2016

Accepted 28 August 2016

Keywords:

On-board diagnostics (OBD)

Engine maps

Vehicle powertrain modelling

Emissions

Portable emissions measurement systems

(PEMS)

ABSTRACT

Air pollution problems persist in many cities throughout the world, despite drastic reductions in regulated emissions of criteria pollutants from vehicles when tested on standardised driving cycles. New vehicle emissions regulations in the European Union and United States require the use of OBD and portable emissions measurement systems (PEMS) to confirm vehicles meet specified limits during on-road operation. The resultant in-use testing will yield a large amount of OBD and PEMS data across a range of vehicles. If used properly, the availability of OBD and PEMS data could enable greater insight into the nature of real-world emissions and allow detailed modelling of vehicle energy use and emissions. This paper presents a methodology to use this data to create engine maps of fuel use and emissions of nitrous oxides (NO_x), carbon dioxide (CO₂) and carbon monoxide (CO). Effective gear ratios, gearbox shift envelopes, candidate engine maps and a set of vehicle configurations are simulated over driving cycles using the ADVISOR powertrain simulation tool. This method is demonstrated on three vehicles – one truck and two passenger cars – tested on a vehicle dynamometer and one driven with a PEMS. The optimum vehicle configuration and associated maps were able to reproduce the shape and magnitude of observed fuel use and emissions on a per second basis. In general, total simulated fuel use and emissions were within 5% of observed values across the three test cases. The fitness of this method for other purposes was demonstrated by creating cold start maps and isolating the performance of tailpipe emissions reduction technologies. The potential of this work extends beyond the creation of vehicle engine maps to allow investigations into: emissions hot spots; real-world emissions factors; and accurate air quality modelling using simulated per second emissions from vehicles operating in over any driving cycle.

© 2016 The Authors. Published by Elsevier Ltd. This is an open access article under the CC BY license (<http://creativecommons.org/licenses/by/4.0/>).

1. Introduction

Emissions of greenhouse gases (GHG) and local air pollutants present persistent challenges in both space and time. The mean, global concentration of GHG must not exceed 450 ppmv by 2100 to limit temperature change to +2 °C, relative to pre-Industrial levels. The corresponding representative concentration pathway (RCP2.6) requires global GHG emissions to fall 40–70%, relative

to 2010 levels, by 2050 and be at or below zero by 2100 [1]. Similarly, noxious air pollution persists in urban areas despite reductions in regulated emissions levels from combustion events accompanying transport movements. Indeed, there were no exceedances of the nitrogen dioxide (NO₂) annual limits in rural areas [2].

Transportation accounted for 20% of CO₂ emissions [3] and 46% of nitrous oxide (NO_x) emissions [2] in the EU-28 in 2013. Euro standards for vehicle emissions were designed to reduce local air pollutant emissions and is part of the broader Clean Air Policy Package. Currently, vehicle emissions in Europe and the US are calculated using distance-based factors under the Computer

* Corresponding author.

E-mail address: jdkb2@cam.ac.uk (J.D.K. Bishop).

URL: <http://www.eeci.cam.ac.uk> (J.D.K. Bishop).

Nomenclature

GHG	greenhouse gases	PEMS	portable emissions measurements system
IPCC	Intergovernmental Panel on Climate Change	OBD	on-board diagnostics
RCP2.6	representative concentration pathway 2.6, is the IPCC climate change mitigation scenario where radiative forcing peaks and falls to 2.6 W/m ² by 2100	NEDC	New European Driving Cycle
CO ₂	carbon dioxide	CO	carbon monoxide
NO _x	nitrous oxides	ADVISOR	advanced vehicle simulator
EU-28	28-member European Union	EA	Emissions Analytics
COPERT	Computer Programme to calculate Emissions from Road Transport	ANL	Argonne National Laboratory
MOVES	Motor Vehicle Emission Simulator	UDDS	Urban Dynamometer Driving Schedule
ANN	artificial neural networks	FTP	Federal Test Procedure
		HWFET	Highway Fuel Economy Test
		ETC or FIGE	European Transient Cycle, for heavy goods vehicles
		SAD	sum of absolute deviations

Programme to calculate Emissions from Road Transport (COPERT) and Motor Vehicle Emission Simulator (MOVES), respectively. COPERT emissions factors are based on average speed, while MOVES uses vehicle specific power which simulates road load. Both methods extract emissions factors from dynamometer data gathered from a subset of vehicles, combined with activity to estimate fleet-level inventories. However, the ability for COPERT and MOVES to predict emissions accurately may be limited by the amount of dynamometer data available on new vehicle powertrain technologies. For example, the latest COPERT emissions factors use data from 81 Euro V vehicles (31 petrol, 50 diesel) and 20 first generation, Euro VI vehicles (1 petrol, 19 diesel) [4], while MOVES emissions factors are based on data from 2.3 million tests from over 500,000 vehicles but only up to calendar year 2005 [5].

Recent analyses show that these laboratory-derived emissions factors based on regulated driving cycles overestimate real-world fuel economy by up to 40% [6] and underestimate emissions of NO_x by an average seven times in modern Euro VI (and equivalent Tier 2 Bin 5 in the US) vehicles [7]. This discrepancy between regulated and real-world emissions is reflected at traffic measurement stations where the highest concentrations of NO₂ (and 93% of all exceedances of the legal annual limit) were observed [2].

A more accurate method for simulating emissions is available but, until now, has lacked data for widespread use. Vehicle dynamic simulation packages, such as the Advanced Light-Duty Powertrain and Hybrid Analysis (ALPHA) tool [8], Autonomie [9] and the Vehicle Energy Consumption Calculation Tool (VECTO) [10], can predict drivetrain power requirements accurately for any driving cycle. However, they require empirical data for the energy use and associated emissions from the fuel-to-power converter (engine). Until recently, empirically-derived engine and emissions maps were not available in large quantities. The most reliable method for obtaining steady-state engine maps is via dynamometer testing which is both time consuming and expensive. Therefore, many maps are not available freely in the literature, leading researchers to simulate the performance of novel vehicle powertrains using old engine maps. Moreover, there are limitations to using steady-state maps generated from dynamometer testing in the transient conditions which characterise real-world vehicle operation [11]. Engine dynamometer testing can be used to create maps based on transient driving cycles. The resulting engine maps may still yield large errors in fuel use and emissions if the transient test cycles do not reflect real-world driving closely. Therefore, the steady-state maps available in the literature may not yield accurate results when researchers use them on driving cycles which differ to what they were generated on.

Two main approaches are used in the literature to determine fuel use and emissions under transient conditions. First, artificial neural networks (ANN) have been used to simulate accurately

changes in engine operation, such as cam phasing [12], octane number [13], fuel blends [14,15] and common rail direct injection with various exhaust gas recirculation strategies [16]. However, accurate results using ANN are achievable because steady-state, dynamometer testing is used to generate the training data. Moreover, not only are ANN approaches best suited to situations where results are steady and repeatable [17], but also the optimum network architecture may vary from one dataset to another [15]. The nature of collecting data while vehicles are driving normally introduces a number of external factors, such as weather and traffic conditions, which eliminate the ability to reproduce results robustly. Therefore, ANN may not be appropriate to generate engine maps using data gathered while driving.

The second approach applies transient correction factors to steady-state maps. Third and fourth order polynomials were developed in Giakoumis et al. [18,19] for each speed point of a heavy-goods vehicle engine with respect to torque. This analytical form was used to predict transient fuel use and emissions of nitric oxide and soot. Exhaust temperature and emissions depend on both instantaneous and historical engine speed and torque demands [11]. Therefore, correction factors were developed based on the difference between exhaust temperatures for hot and cold operation at each engine load and speed point. The development of correction factors requires a base steady-state map which is obtained typically from dynamometer testing.

In contrast to both the regulatory and academic approaches discussed, this work presents a novel methodology to create engine maps of real-world fuel use and emissions of both GHG and local air pollutants based on data collected from on-board diagnostics (OBD) and portable emissions measurement systems (PEMS) when driving under real-world conditions. Therefore, this work could be adopted within COPERT and MOVES, the use of which is required by nearly every country and state in the developed world to estimate emissions. PEMS have been used extensively in recent times to understand the emissions from vehicles under real-world driving conditions. However, the on-board measurements do not provide the same quality of data as lab-based measurements on account of variability in driving [20], ambient conditions and the accuracy of measuring certain pollutants on the go. In most cases, the PEMS results are analysed and compared to the Euro emissions limits [21–24]. PEMS results have also been compared to the performance of the vehicle on a chassis dynamometer under type approval settings and the New European Driving Cycle (NEDC) [25–27].

Regulations in the European Union [28] and United States [29] require OBD and PEMS be used to verify in-use emissions from heavy-duty vehicles. This approach is expected to be extended to light duty vehicles, beginning in Europe through the Real-Driving Emissions test [30]. The requirement of PEMS testing through an

in-service conformity procedure will yield large amounts of data across a range of vehicles. The methodology presented in this paper is designed to exploit the large data sets which are expected to become available from widespread PEMS testing. Developing engine maps for each vehicle in the fleet will enable more nuanced modelling of energy use and emissions at multiple spatial (country, city and roadway) and temporal (year, day and second) scales.

This work presents a novel way to simulate accurately the energy use and associated greenhouse gas and local air pollution from engines. Our approach sits at the intersection of innovation, research and development and its accuracy is demonstrated at the per second and trip level. The method presented in Section 2 describes the creation of gearbox models and sets of candidate engine maps which are tested on a range of vehicle configurations. The optimum map for each of fuel use and emissions is the one with the smallest sum of absolute deviations across each second of the respective time series.

2. Method

A schematic of the method is given in Fig. 1 and comprises four parts: the first describes how the effective gear ratio and gear shift regime is derived from the OBD data; the second gives the procedure for developing the engine maps for each output of fuel use and emissions of NO_x , carbon dioxide (CO_2) and carbon monoxide (CO); the third describes how the gearbox model and candidate engine maps are combined with vehicle physical characteristics in the ADVISOR powertrain simulation environment; and the fourth investigates the sensitivity of the outputs to vehicle physical characteristics. A seven-second, one dimension median filter was applied to smooth engine speed, wheel speed and the outputs.

The robustness of this method is demonstrated across three vehicles, full details of which are given in Table 1:

1. A DAF CF 75 tractor unit tested on a dynamometer as a combination vehicle under 20 t load reporting exhaust temperature,

Table 1

Physical characteristics of ANL Chevrolet Cruze, EA Volkswagen Golf and DAF CF 75 vehicles used to demonstrate methodology. Asterisks indicate ADVISOR default or assumed values.

Attribute	Chevrolet Cruze	Volkswagen Golf	DAF FT CF 75
Test mass (kg)	1731	1300	20,000
Coefficient of drag, Cd	0.34	0.31	0.6*
Frontal area (m^2)	2.1	2.2	9.7
Wheelbase (m)	2.7	2.6	8*
Top gear number	6	5	12
Transmission	Automatic	Manual	Automatic
Coefficient of rolling resistance, Crr	0.009*	0.009*	0.0059
Max engine torque (Nm)	358	320	1275
First engine speed at max torque (RPM1)	2000	1750	1100
Second engine speed at max torque (RPM2)		3000	1700
Max engine power (kW)	110	110	228
Torque at max engine power (Nm)	263	300	990
Engine speed at max power (RPM1)	4000	3500	2200

fuel use and emissions of NO_x , CO_2 , CO and particulates at engine-out and the tailpipe.

2. A Volkswagen Golf diesel vehicle tested by Emissions Analytics (EA) using a SEMTECH-DS PEMS reporting exhaust temperature, fuel use and tailpipe emissions of NO_x , CO_2 and CO.
3. A 2014 Chevrolet Cruze diesel vehicle tested on a chassis dynamometer at the Argonne National Laboratory (ANL) [31] reporting only fuel use across a number of driving cycles with hot and cold starts.

Data post-processing from the DAF and EA tests and ADVISOR output data at 1 Hz. The output from the ANL test is reported at 10 Hz and interpolated to 1 Hz. This lower frequency aligns with the velocity-time inputs used in the driving cycle simulation. The simulation is assumed quasi steady-state where the engine operates in steady-

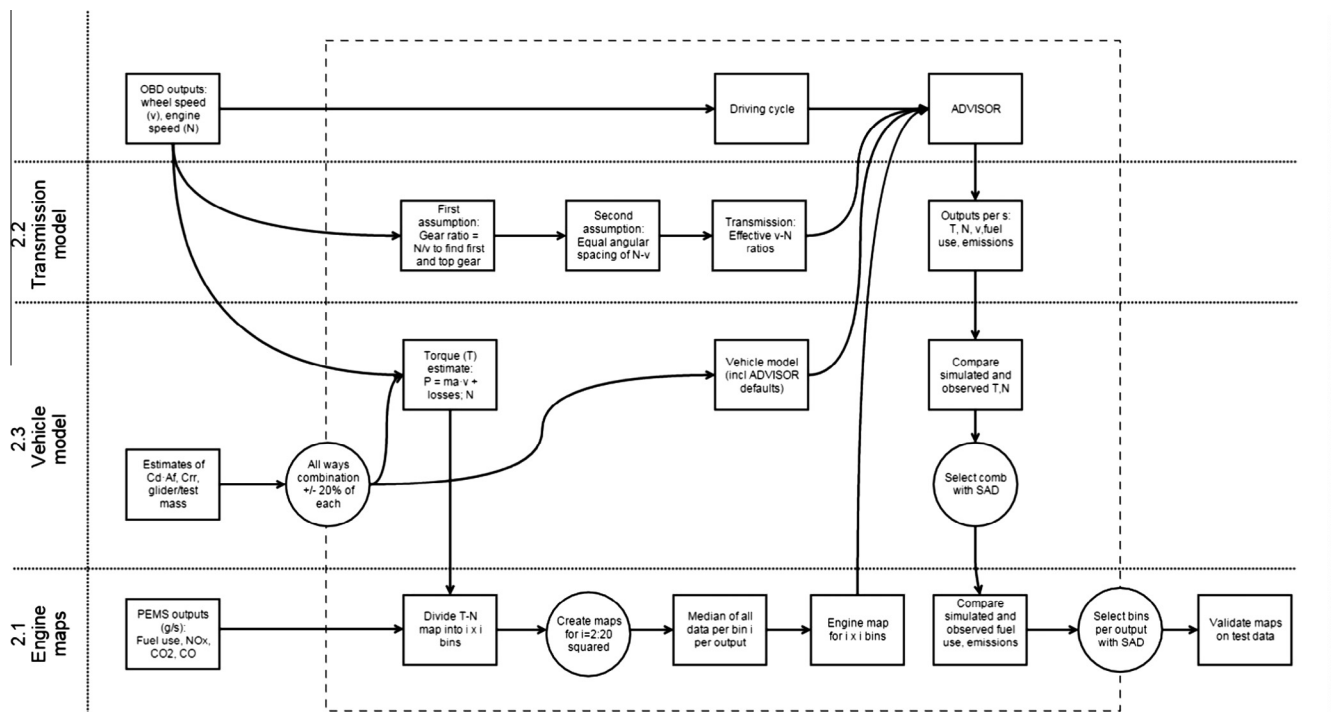


Fig. 1. Schematic of method to create engine maps of transient fuel use and emissions. The dotted lines show which the parts of the model which correspond to engine maps, vehicle modelling and transmission modelling and use the same numbering as is presented in the methodology text. The dashed line encloses the full method.

state for each second in the driving cycle. Additionally, 1 Hz time resolution is the maximum for some of the on-board sensors. Therefore, measuring faster transients may require more advanced equipment and preclude the use of real-world data collection. Returning to the lab reintroduces the challenges which this method seeks to overcome. Additionally, modifications to the driving cycle simulation would be required to account for the finer time steps.

2.1. Creating candidate engine maps

Steady-state engine maps of fuel use and emissions are created when the measured values are stable at each engine speed-torque point. Under real-world driving, a range of values will occur at the same engine speed-torque point. However, a single value must be used to represent the output at each point in the engine map.

The fuel use and emissions data was separated into bins to determine a representative value at each engine speed-torque point to develop a map. The engine speed and torque range was divided into an equal, evenly-spaced number of bins. Data was allocated to the bins which they were closest to. To determine the number of bins to best represent the range of operating conditions, a system optimum was sought. A small number of bins would be expected to contain data over a large range of values. Alternatively, a large number of bins might only have one or two data points each. Fig. 2 illustrates the distribution of data in different bins, using fuel use by the DAF CF 75 as an example. The mean of the data in each bin was used.

It could not be known *a priori* how many bins were necessary to reconstruct accurately the map for each output. Therefore, a set of candidate engine maps was produced for each output using from 2^2 to 10^2 bins. The maximum torque envelope for each engine was constructed from the vehicle manufacturer specifications, where possible. The envelope comprised three engine speed points: the minimum (RPM1) and maximum (RPM2) speeds which returned peak engine torque; and the engine speed (RPM3) where maximum power occurred. If RPM1 was reported only, RPM2 was set as the median of RPM1 and RPM3. The maps were created using

observed driving data only. That is, we did not extrapolate a fuel use or emissions value for a part of engine speed-torque space where no driving occurred. Therefore, obtaining complete maps requires data be collected from the vehicle operating under a range of driving conditions.

Engine maps using tailpipe emissions, such as are available from conventional PEMS testing, internalise the effects of any emissions reductions technologies present in the tailpipe. Maps developed using engine-out data are independent of emissions reductions technologies in the tailpipe.

2.2. Deriving effective gear ratios and shift procedure

The gearbox transmits power through the drivetrain by translating the torque and speed generated by the engine to a different applied torque and speed at the wheels. Accurate conversion of wheel speed to engine speed through the transmission and differential is essential to ensure that the simulated engine operation aligns with the observed torque-speed points for each second of the driving cycle. The open OBD channels may not report the gear number corresponding to the wheel speed in each second of the driving cycle. Similarly, the final drive ratio and wheel radius may not be reported for all vehicles. Therefore, the transmission encompassing the wheel radius, final drive ratio and gearbox must be estimated.

The effective gear ratio represents the unique, combined effect of the wheel radius, final drive ratio and gearbox and is the quotient of engine speed and wheel speed. The effective ratio of each gear can be represented as a line of fixed gradient on a wheel speed-engine speed plot. Plotting all gears resembles a set of “fingers.” The second, refined estimate of gear ratios assumed the “fingers” swept an arc from first gear to top gear, with even spacing between the gears. The tangent of the angle gave the rise and run to calculate the gradient, corresponding to the gear ratio. Each engine/wheel speed data point was assigned to closest gear based on minimum absolute distance.

An engine speed-torque shift envelope was identified for each gear using the data assigned to that gear. Such an envelope is used to determine when the gearbox should shift up or down to keep the engine operating in a particular speed-torque region. Minimum speed to shift down was the maximum of the engine idle speed or the 5th percentile of the engine speeds observed for that gear. Maximum speed to shift up was the 95th percentile value. These percentiles were chosen to avoid outliers which might push the shift boundaries far from main data set. The first point in the shift up envelope was the engine idle speed which follows better the contours of the data in each gear.

2.3. Vehicle simulations to reconstruct emissions on a per second basis

The ANL dynamometer tests cover a range of vehicle operating conditions, including the main Urban Dynamometer Driving Schedule (UDDS), Federal Test Procedure (FTP), Highway Fuel Economy Test (HWFET), high speed and aggressive US06 driving cycles. Cold and hot starts are investigated at a range of ambient temperatures and air conditioning loads. These driving cycles are illustrated in Barlow et al. [32] and data was collected at 10 Hz. Full drive schedules at 1 Hz, 10 Hz and supporting information are available from the US Environmental Protection Agency [33]. A linear interpolation was performed on the 10 Hz ANL test data at 10-s intervals to return a 1 Hz time series.

The DAF FT CF75 310 4 × 2 day cab tractor unit used a PR 228 kW [34], 1275 Nm Euro V engine [35] and 12-speed 12AS1420 gearbox [36] and is driven on the European Transient, or FIGE, Cycle [32,37]. The DAF CF 75 was tested under load conditions to simulate a combination vehicle with overall vehicle mass

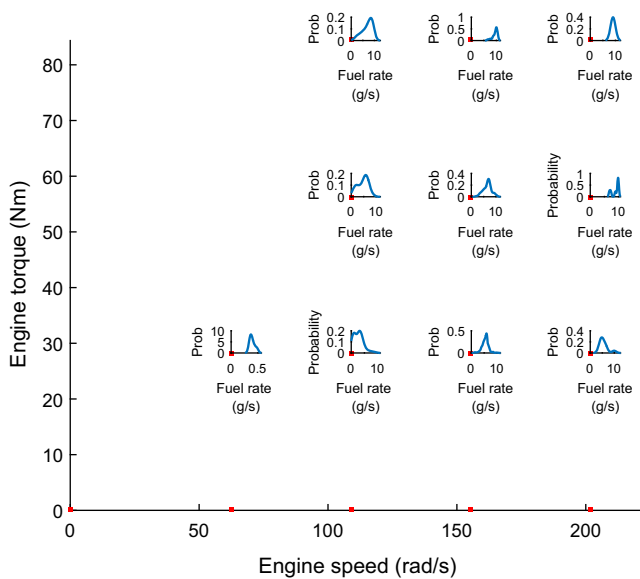


Fig. 2. Probability distribution function of fuel use (g/s) by the DAF CF 75 in each bin when the engine speed-torque map is divided into 25 bins (5 × 5). Red squares denote the (0,0) coordinate of each bin. The x-axis in each subplot is the fuel use and the y-axis is the probability of achieving that value. (For interpretation of the references to color in this figure legend, the reader is referred to the web version of this article.)

of 20 t. The frontal area and wheelbase values given in Table 1 represent those of a typical tractor and trailer [38].

The Volkswagen Golf diesel was driven on the 80 km EA test route west of London which comprises motorway and non-motorway driving sections.

Models of the vehicles were developed using ADVISOR version 2003-00-r0116 on Matlab R2016b which integrated the derived gearbox, candidate engine maps and vehicle characteristics to reconstruct the observed outputs on a per second basis. Physical characteristics of the vehicles were taken from manufacturer specifications, where available. The mass of the Volkswagen Golf lies at the high end of the range of 2012 vehicle masses recorded across the trim levels [39]. Test mass, coefficient of drag and rolling resistance for the ANL Chevrolet Cruze were derived from coast down data [31]. In other cases, the ADVISOR default values were used. Full specifications using in the modelling is given in Table 1.

The method of extracting gear ratios internalised wheel size and final drive ratios. Therefore, these were set to 1 in the appropriate powertrain submodels. The routine loaded the candidate maps for fuel use and each of the emissions for a given number of bins. The wheel speed was loaded as the driving cycle over which the vehicle was simulated in ADVISOR. The simulation outputs were fuel use and emissions for each second and the distance travelled over the driving cycle.

2.4. Sensitivity of fuel use and emissions to vehicle physical characteristics

Engine torque was calculated as most vehicles do not report it on the OBD channels. The ADVISOR default powertrain losses of 8% were assumed in the absence of data on losses as a function of gear number and other variables. Therefore, the power developed at the engine shaft was 108% of that transferred to the wheel, $T_{engine} \cdot \omega_{engine} = 1.08 \cdot m \cdot VSP$, where: T_{engine} = output torque from engine; ω_{engine} = output engine speed; m = vehicle mass; and VSP = vehicle specific power [40], given by:

$$VSP = v \cdot a + \frac{1}{2} \cdot \rho_{air} \cdot C_d \cdot \frac{A_f}{m} \cdot v^3 + (C_{rr} + \sin(\theta)) \cdot g \cdot v \quad (1)$$

where v = wheel speed, m/s; a = acceleration, m/s²; ρ_{air} = density of air, 1.2 kg/m³; C_d = coefficient of drag; A_f = frontal area, m²; C_{rr} = coefficient of rolling resistance; g = acceleration due to gravity, 9.81 m/s²; and θ is the angle of inclination between two consecutive data points, radians. The DAF CF 75 and ANL Chevrolet Cruze were both tested on dynamometers with zero road grade. The engine torque demand calculated for the EA Volkswagen Golf included the change in road grade associated with real-world driving. In all cases, no measurement of wind speed was available. Therefore, wind speed was set to zero in all cases. Internal friction losses were not considered.

In general, the physical characteristics relating to power loss – coefficient of drag, frontal area and tyre rolling resistance – are not provided in the literature and must be assumed. Accurate values of both the power required at the wheel and the gearbox are necessary for the simulated engine torque-speed per second to be close to the observed values. Therefore, the sensitivity of the ADVISOR outputs to the characteristics of each vehicle was investigated. Effective drag (the product of coefficient of drag and frontal area) and rolling resistance were varied each by $\pm 10\%$ in 10% increments. Test mass was varied by $\pm 20\%$ in 10% increments to recognise the wider range of possible values. The sweep was conducted on all combinations of these three characteristics which yielded 125 unique vehicle configurations plus the base case.

2.5. Selecting the optimum vehicle configuration and engine maps

ADVISOR was run once for each vehicle configuration and simulated engine torque and speed achieved for each second saved. This pair of vectors was compared to the observed data in corresponding time steps and the Euclidean distance between each calculated. The optimum configuration returned the smallest sum of absolute deviations (SAD) which was used because it is robust to outliers. Conversely, large differences between observed and simulated data would affect the output if squared errors were used.

ADVISOR uses a two-dimensional interpolation of each fuel and emissions map, indexed by engine torque and speed to determine the corresponding output for each second. Therefore, a two-dimensional interpolation of engine torque and speed was performed at each second for the optimum vehicle configuration across the set of candidate engine maps, using from 2² to 10² bins, for each output. It was not assumed that engine maps of fuel use and emissions should use the same number of bins. Therefore, the optimum bin number for each output corresponded to the timeseries with the smallest SAD between observed and simulated values in each second using the optimum vehicle configuration.

2.6. Validating engine maps

The final aspect of the method involves validating the engine maps on a new driving cycle. This validation was only possible for the Chevrolet Cruze because data was available for a large number of driving cycles. Therefore, the UDDS and HWFET driving cycles were used to create the engine maps. The Chevrolet Cruze was simulated driving on the US06 as the validation driving cycle using the effective gear ratios, optimum vehicle configuration and these engine maps. Shift envelopes were re-calculated for the validation data under the assumption that gear shifts will depend on the driver's attempts to meet the driving cycle velocity in each second, particularly for vehicles with manual transmissions.

The method described has advantages over similar work which tries to create engine maps from empirical data. Namely, both Fontaras et al. and Kousoulidou et al. filter out data considered highly transient [23,41] and use ADVISOR to simulate their vehicles. Fontaras et al. used 10 bins for the fuel map, while Kousoulidou et al. used a number of extrapolations to create their engine maps. Conversely, we use the optimum number for each of fuel use and individual emissions species to maximise accuracy on a per second basis. Moreover, the method is robust to vehicle type because it extracts effective gear ratios and sweeps through vehicle physical characteristics.

3. Results and discussion

The results of the method applied to the DAF CF 75, Volkswagen Golf and Chevrolet Cruze, are presented in this order. Each results section comprises a discussion on the gearbox development, the selection of the optimum vehicle configuration and the optimum engine maps. Time series of observed and simulated outputs are presented.

3.1. DAF CF 75 as 20 t combination vehicle

Fig. 3 illustrates how the effective gear ratios were determined using the speeds of the engine and wheels. Fig. 3a shows the initial estimate of gear ratios based on the assumed shift points and corresponding speed of engine and wheel. The “fingers” in Fig. 3b were used as the basis for fitting the lines of Fig. 3c on the assumption of even spacing of angles. The shift envelopes for the DAF CF

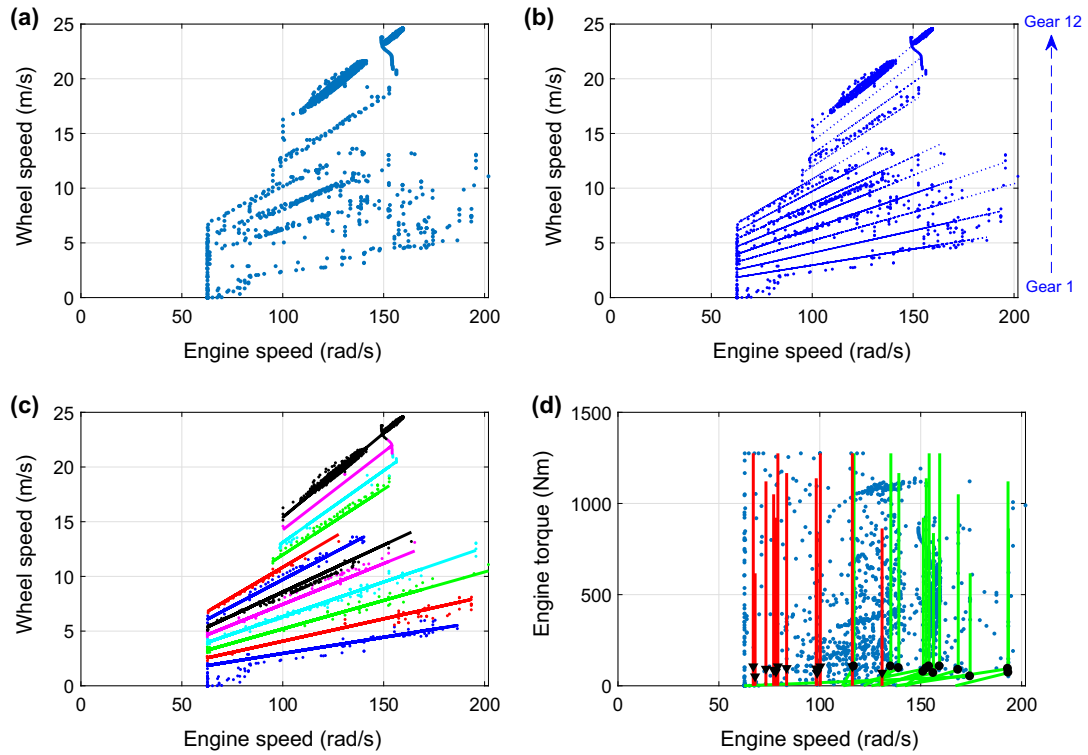


Fig. 3. (a) Scatter of data by engine speed and wheel speed and illustrating “fingers” corresponding to the vehicle operating in the same gear. (b) Dotted lines representing evenly spaced angles between top gear (gear = 12) and first gear. (c) Overlay of new effective gear ratios (lines of constant gradient) with observed data, coloured to match the assumed gear. (d) Shift up (green) and down (boundaries) for each gear as vertical lines through the respective peaks of the probability distribution functions for each gear. (For interpretation of the references to color in this figure legend, the reader is referred to the web version of this article.)

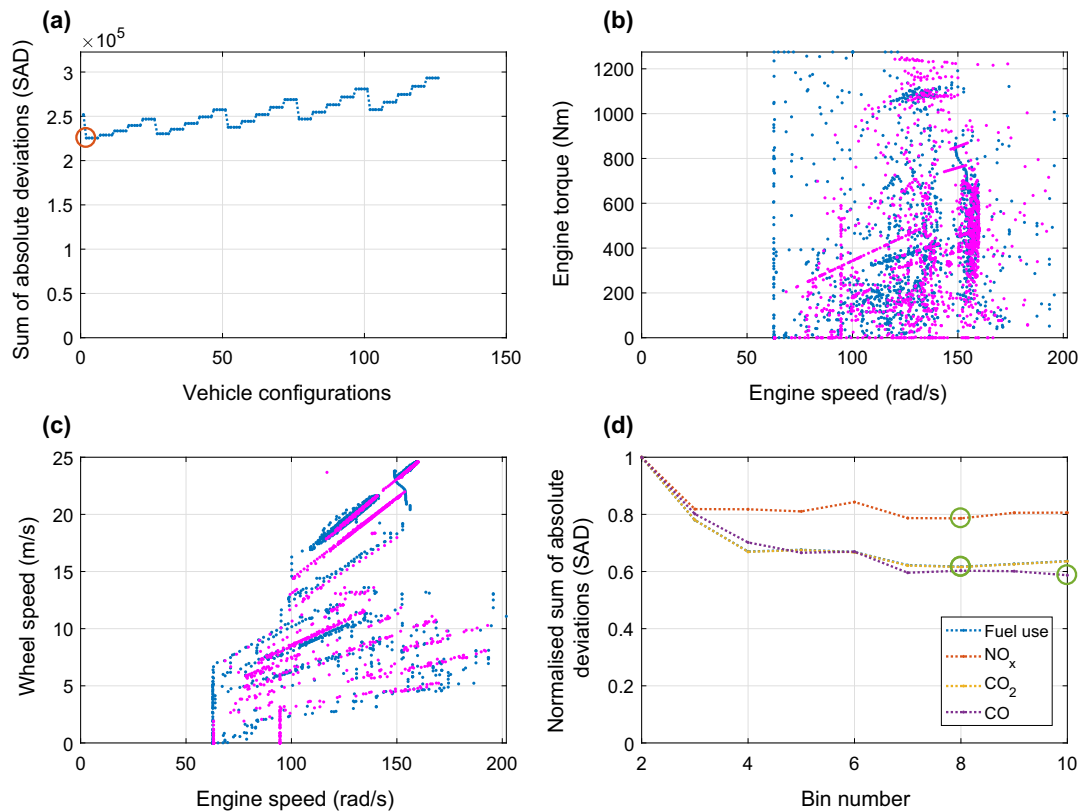


Fig. 4. (a) Sum of absolute deviations between each observed engine torque-speed pair and those of the 126 unique vehicle configurations. Orange circle represents the unique vehicle configuration with the smallest SAD. (b) Scatter of observed engine torque-speed (blue) and simulated (magenta) using the optimum vehicle configuration. (c) Scatter of observed wheel-engine speed (blue) and simulated (magenta) using the optimum vehicle configuration. (d) Sum across time series of absolute deviations per second between observed and simulated fuel use and emissions across bin numbers from two to 10 which is normalised to the maximum value of each output. Green circles indicate the bin numbers with smallest SAD for each output. (For interpretation of the references to color in this figure legend, the reader is referred to the web version of this article.)

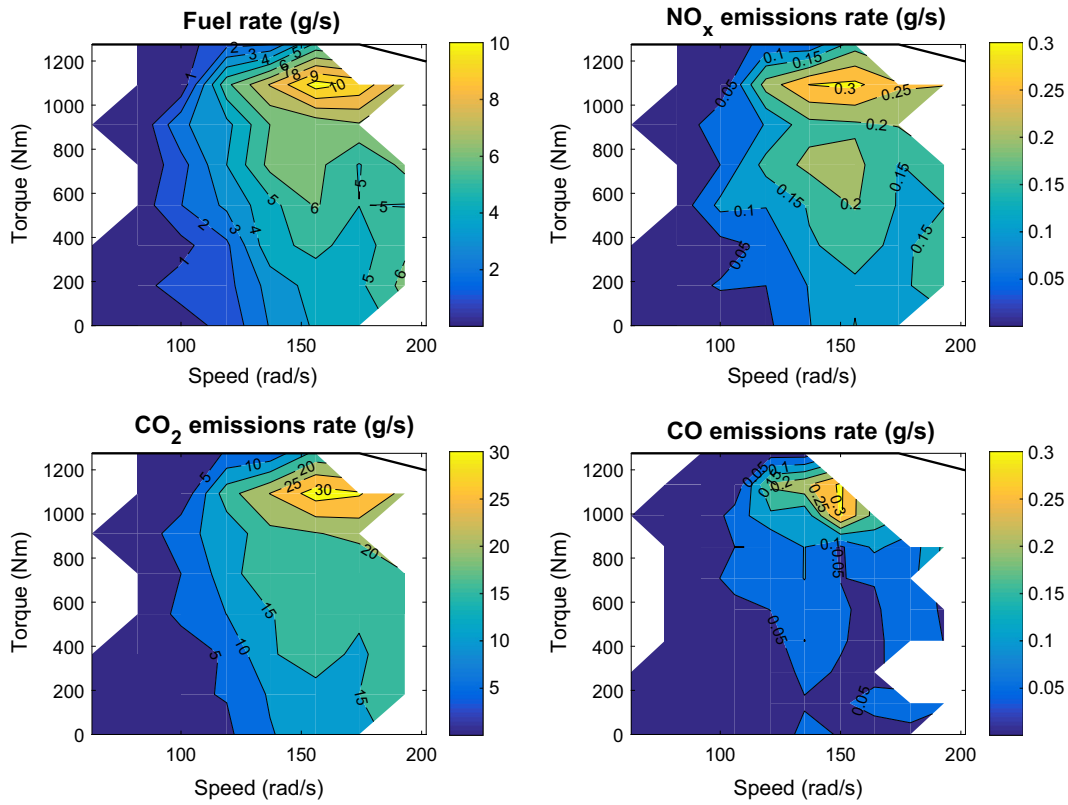


Fig. 5. Engine maps of transient fuel use and engine-out emissions of NO_x, CO₂ and CO created using the optimum bins for the DAF CF 75. The black lines represent the maximum torque envelope.

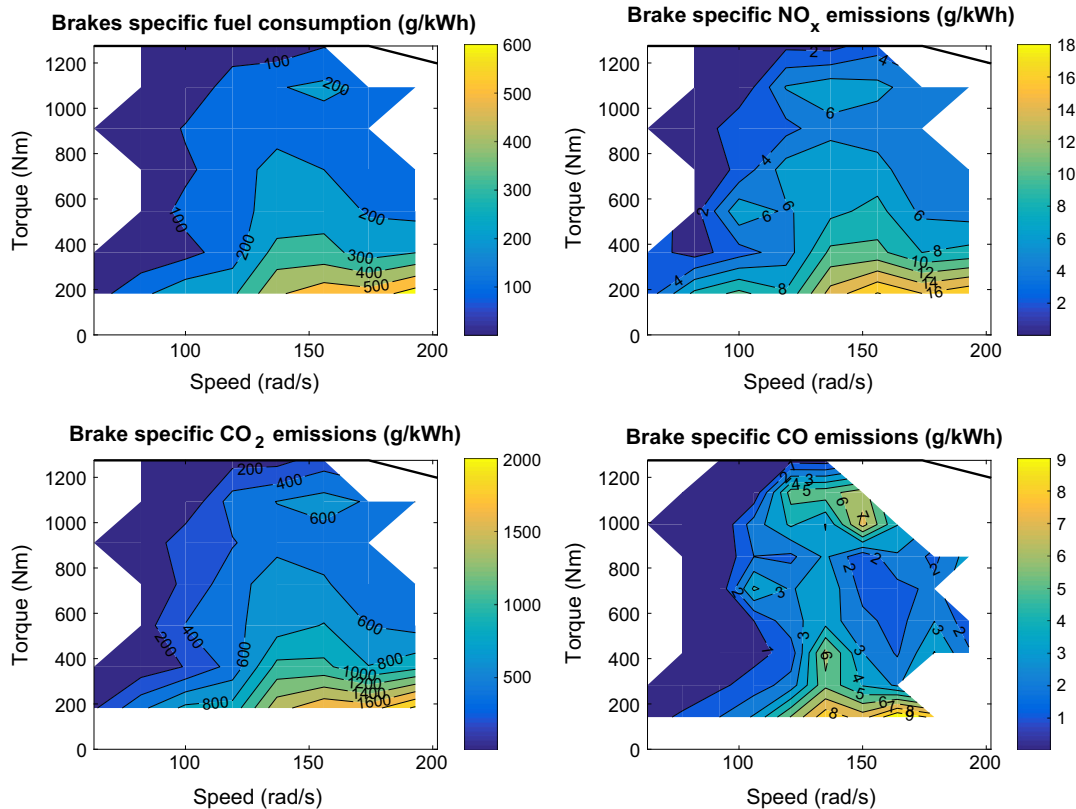


Fig. 6. Engine maps of transient brake specific fuel use and engine-out emissions of NO_x, CO₂ and CO (g/kWh) created using the optimum bins for the DAF CF 75. The black lines represent the maximum torque envelope.

75 are presented by 24 lines, a shift up and shift down pair for each of the 12 gears in Fig. 3d.

The derived gearbox was combined with the vehicle's physical characteristics for each of the 126 combinations of vehicle configurations (different physical constants) and simulated in ADVISOR. Fig. 4a illustrates the sum of absolute deviations per second of Euclidean distance between observed and simulated engine torque-speed pairs across the vehicle configurations. The orange circle corresponds to configuration 2 which returned the smallest SAD and was chosen as the optimum configuration. The DAF CF 75 combination vehicle with this configuration had effective drag of 4.9 m², a glider mass of 4600 kg and rolling resistance coefficient of 0.0053.

Fig. 4b and c shows the observed engine torque-speed scatter in blue and the simulated output at the optimum vehicle configuration in magenta. The method as described reproduces most of the observed torque-speed points in the central cluster at engine speeds of 100–160 rad/s. Simulated torque-speed points do not reproduce the low speed (63 rad/s), medium to high torque (greater than 500 N m) points. Likewise, the absence of magenta points at low wheel speed (less than 5 m/s), high engine speed in Fig. 4c suggests the truck skipped low gears in the simulation. The aim of ADVISOR is to match wheel speed to the speed demanded by the driving cycle in each second. In some cases, multiple gear options may satisfy this requirement, leading to a discrepancy between simulated and observed gear choice.

Fig. 4d shows the sum over the time series of absolute deviations per second for fuel use (blue) and emissions of NO_x (orange),

CO₂ (yellow) and CO (purple) across the bin numbers from 2² to 10². Green circles indicate the number of bins with the minimum SAD for each of the outputs: 8² each for fuel use and emissions of NO_x and CO₂; and 10² for CO emissions. A more sophisticated, adaptive binning technique was investigated recognising the data was distributed non-uniformly throughout the map. Here, the bin width was inversely proportional to the density of the data, such that wider bin widths were used for areas of sparse data and narrower bins widths used where the data was more dense. However, the simple approach of equal bin widths yielded more accurate results and was used in this work.

Figs. 5 and 6 show the engine maps of fuel use and emissions for the DAF CF 75, on instantaneous and brake specific basis, respectively. These maps display an operating point corresponding to maximum output surrounded by isocontours of constant output. Maximum fuel use and emissions (g/s) occurred at 130–140 rad/s and 1000–1200 N m. Multiple regions of high instantaneous and brake specific NO_x, CO₂ and CO emissions are observed in addition to the operating point of maximum emissions for each pollutant. The blank areas represent regions of engine operation not visited during the driving cycle. The method does not extrapolate parts of the map for which no data exists. Therefore, the most complete maps will be derived from data collected under driving conditions which use the full range of engine operation.

The ETC comprises three sections which represent urban, rural and motorway driving. Fig. 7 illustrates the accuracy of the method at reproducing the outputs per road type. The method reproduced well both the shape and magnitude of fuel use and associated

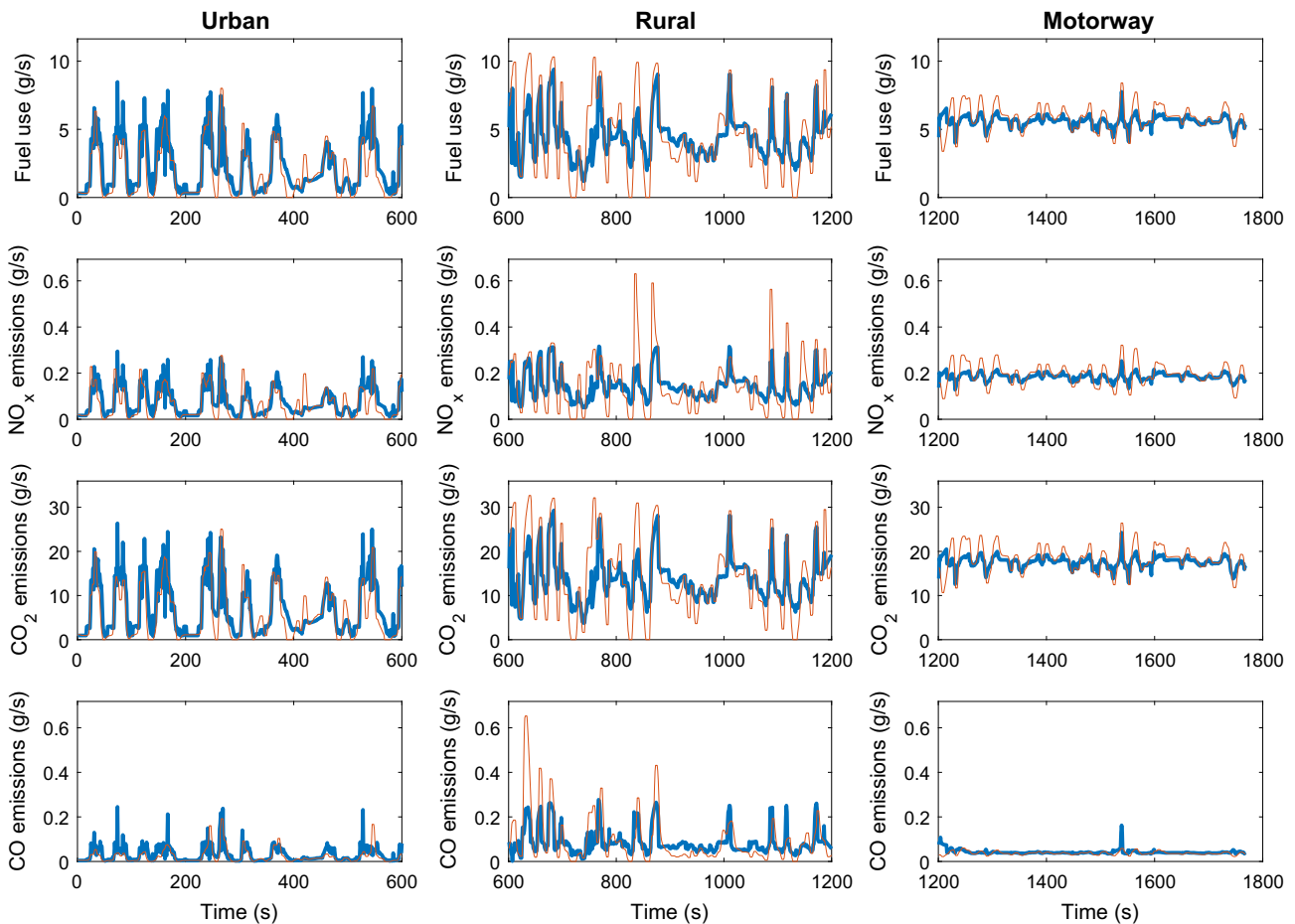


Fig. 7. DAF CF 75 observed (orange) and simulated (blue) mass of engine-out (a) fuel use; (b) NO_x emissions; (c) CO₂ emissions; (d) CO emissions using optimum bins. (For interpretation of the references to color in this figure legend, the reader is referred to the web version of this article.)

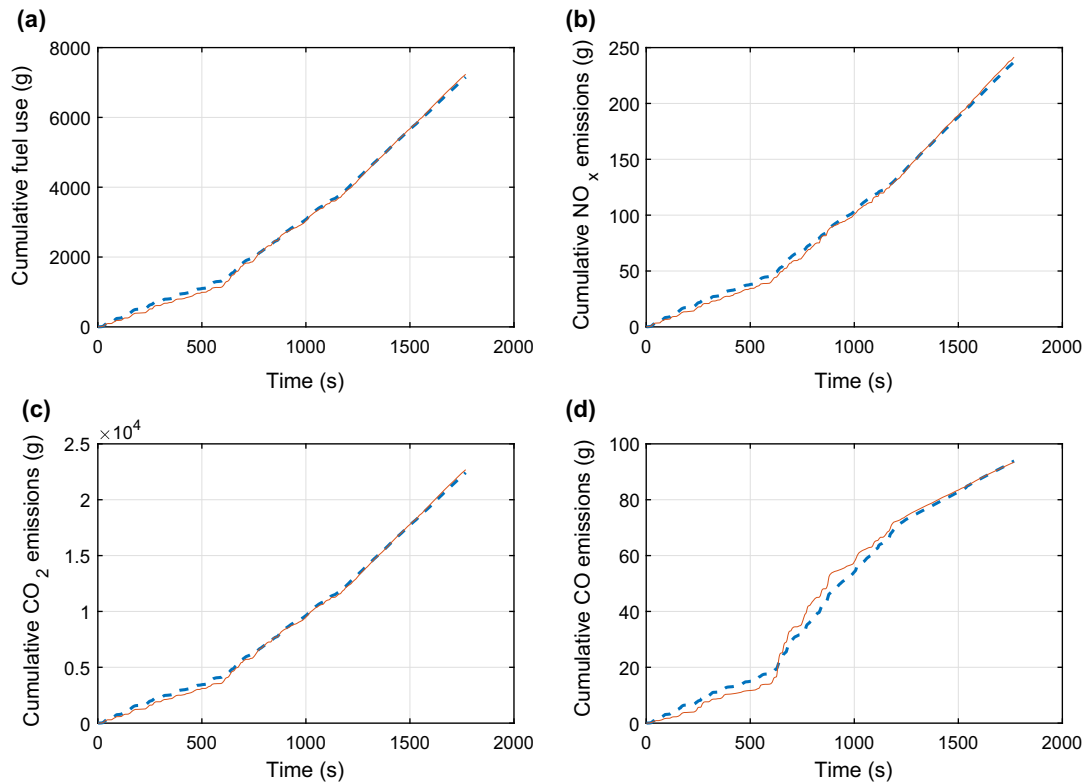


Fig. 8. DAF CF 75 cumulative sum of observed (orange) and simulated (blue) mass of outputs using optimum bins for each output: (a) fuel use; (b) NO_x emissions; (c) CO_2 emissions; (d) CO emissions. (For interpretation of the references to color in this figure legend, the reader is referred to the web version of this article.)

emissions for urban and motorway driving. This implies our methods of extracting the vehicle's physical characteristics, effective gear ratios and transmission control are fit for purpose. In the rural driving particularly, the method reproduced accurately the peaks in per second fuel use and emissions. However, some dips were not simulated as well across the various outputs because the optimum number of bins for reducing SAD across the entire time series returned higher instantaneous fuel use and emissions values at low engine torque values. A different number of bins may have yielded maps which simulated the dips better, but introduced greater errors elsewhere in the time series. This method reproduced fuel use on a per second basis more accurately than the map created by Fontaras et al. [41]. In particular, their model does not capture the higher frequency oscillations of fuel use due to power demand. Kousoulidou et al. show only mean accuracy at the trip level, rather than the accuracy at recreating per second fuel use and emissions [23]. This method outperforms the results in Kousoulidou et al. for CO emissions.

Fig. 8 illustrates the cumulative sum of the four outputs which shows the discrepancy between the observed and simulated values. The simulated values underestimated fuel use and emissions of NO_x and CO_2 by 1.2%, 1.8% and 1.2%, respectively. CO emissions were overestimated by 0.43%. Deviations between fuel use and emissions of NO_x and CO_2 occurred in during urban driving (the first 600 s). The error between observed and simulated CO emissions was more constant across the driving cycle.

Engine-out and tailpipe emissions data was available for the DAF CF 75. One advantage of this data-driven methodology is that maps can be created of emissions on either side of any after treatment emissions reduction technology to isolate its effects. The optimum number of bins for the tailpipe emissions of NO_x , CO_2 and CO were 8^2 , 8^2 and 7^2 , respectively, using the optimum DAF CF 75 configuration and effective gear ratios obtained earlier.

Fig. 9 shows how these maps recreated the observed tailpipe emissions accurately. The absolute error between observed and simulated emissions of NO_x , CO_2 and CO was 1.2%, 0.56% and 7.1%, respectively.

Fig. 10a and b shows the NO_x emissions map at engine-out and at the tailpipe, respectively. The difference of these maps isolated the influence of any tailpipe emissions reduction technologies and is shown in Fig. 10c. The technologies in the truck exhaust succeed in reducing peak NO_x emissions by 51% from 0.3 g/s at 140 rad/s and 1100 N m to 0.15 g/s. The new tailpipe NO_x peak was 0.21 g/s at 160 rad/s and 1100 N m. However, technologies maximise their influence by reducing emissions effectively at the speeds and torques which the engines operate in most. Fig. 10d shows the proportion of time spent in each part of the map. Over the ETC, the engine spent 20% of time operating at 160 rad/s and 550 N m. The influence of exhaust after treatment technologies at this engine operating point was to reduce NO_x emissions by 48% from 0.2 g/s to 0.11 g/s.

NO_x and particulate emissions have the largest direct impacts on human health [42–44]. This method was applied to the particle mass data collected during the DAF CF 75 test. Cumulative particulate mass obtained using the simulation was within 1.5% of the observed values. The largest deviation between simulated and observed emissions occurred during rural driving (600–1200 s). The map of particulates used 8^2 bins and is given in Fig. 11.

3.2. EA Volkswagen Golf

The EA Volkswagen Golf had five gears. Similar to the DAF CF 75, the estimates of the first and top gear ratios were used to determine the intermediate gears. Likewise, the shift envelopes per gear were extracted based on the peak of the probability distribution

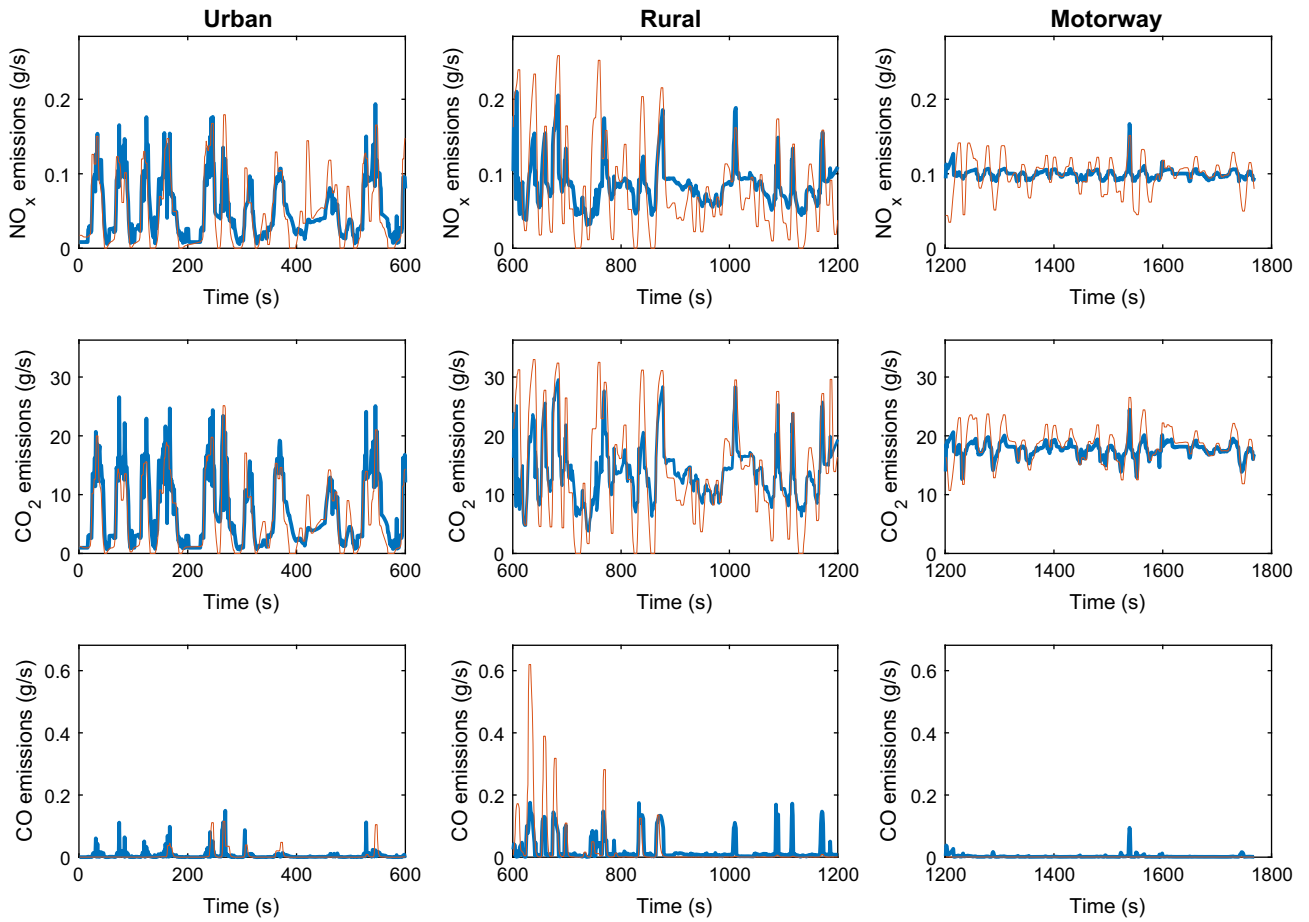


Fig. 9. DAF CF 75 observed (orange) and simulated (blue) mass of tailpipe NO_x emissions, CO₂ emissions and CO emissions using optimum bins. (For interpretation of the references to color in this figure legend, the reader is referred to the web version of this article.)

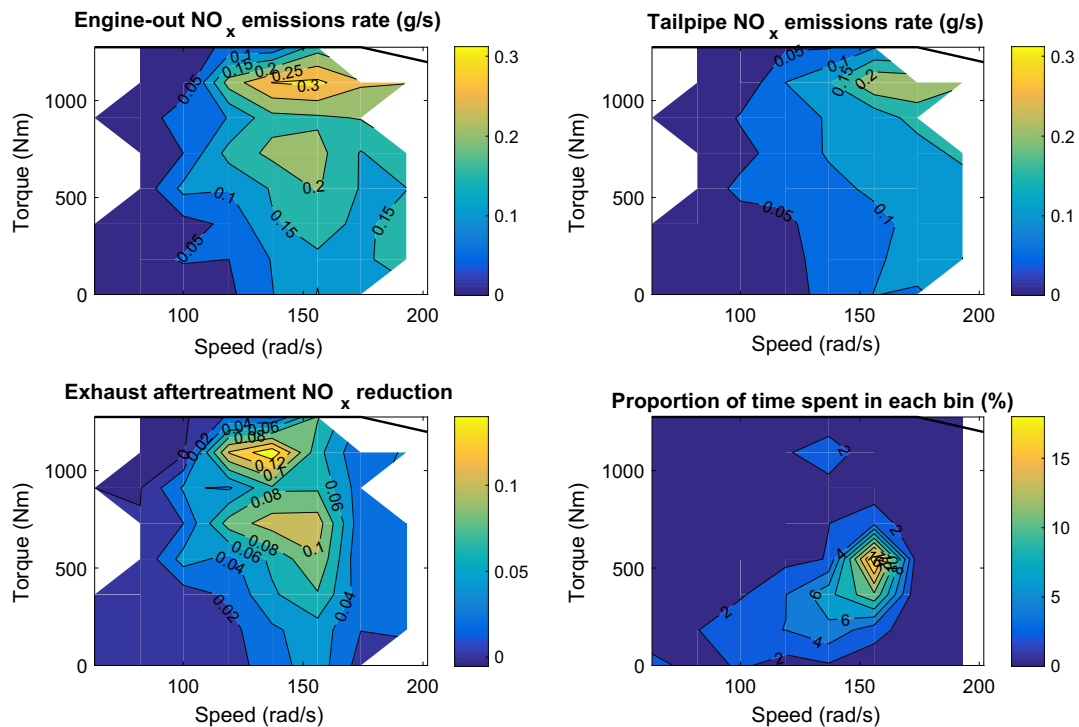


Fig. 10. Maps showing the influence of exhaust after treatment technology on engine-out emissions of NO_x for the DAF CF 75. The black lines represent the maximum torque envelope.

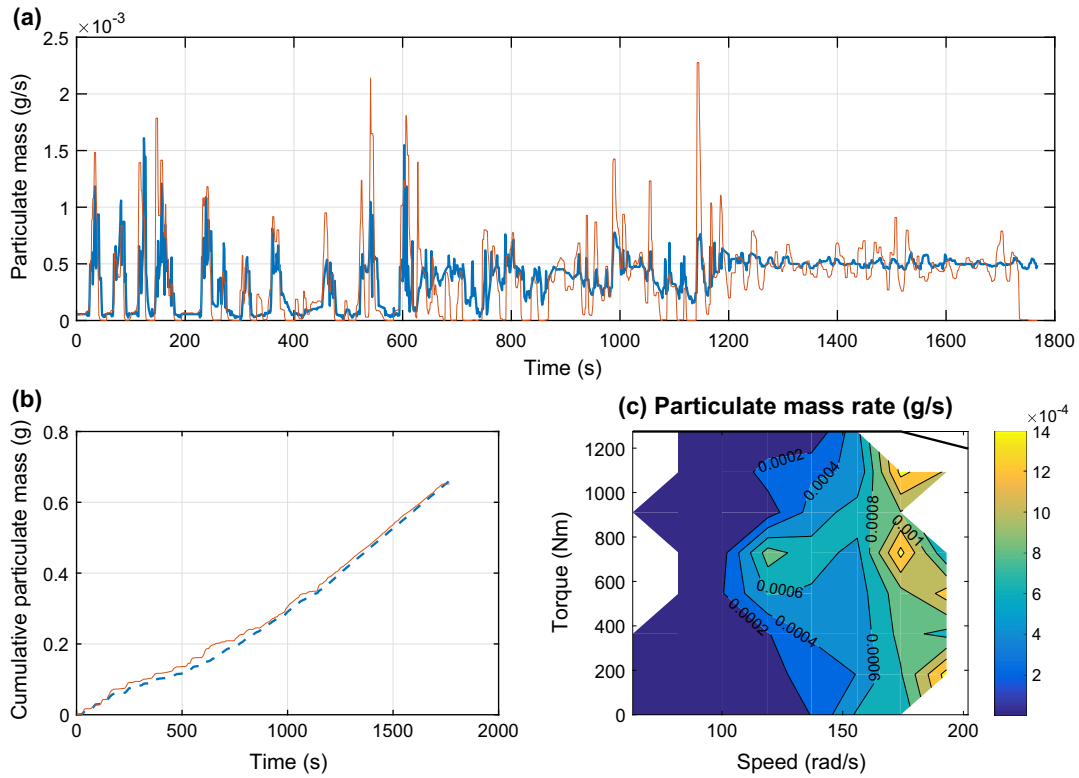


Fig. 11. (a) Observed (orange) and simulated (blue) particulate mass emissions over the ETC. (b) Cumulative sum of observed (orange) and simulated (blue) particulate mass emissions. (c) Engine map of transient particulate mass emissions created using the 8² bins for DAF CF 75. The black line represent the maximum torque envelope. (For interpretation of the references to color in this figure legend, the reader is referred to the web version of this article.)

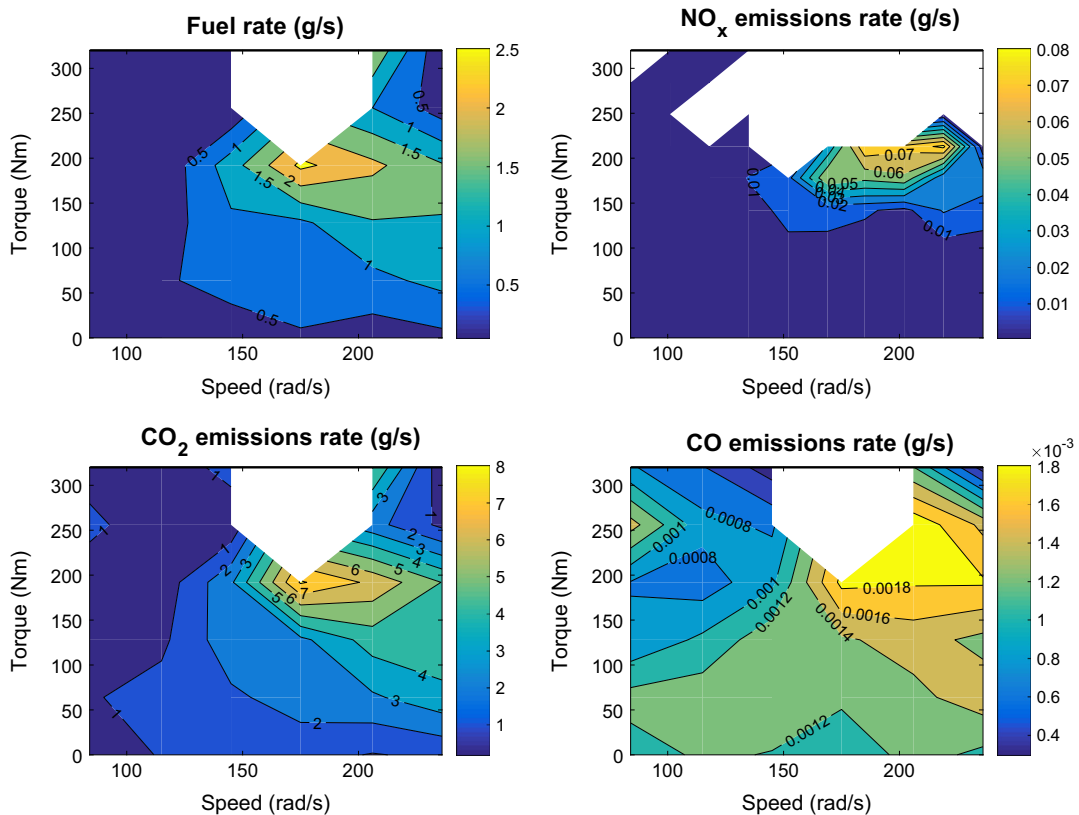


Fig. 12. Engine maps of transient fuel use and emissions of NO_x, CO₂ and CO created using the optimum bins for the EA Volkswagen Golf. The black lines represent the maximum torque envelope.

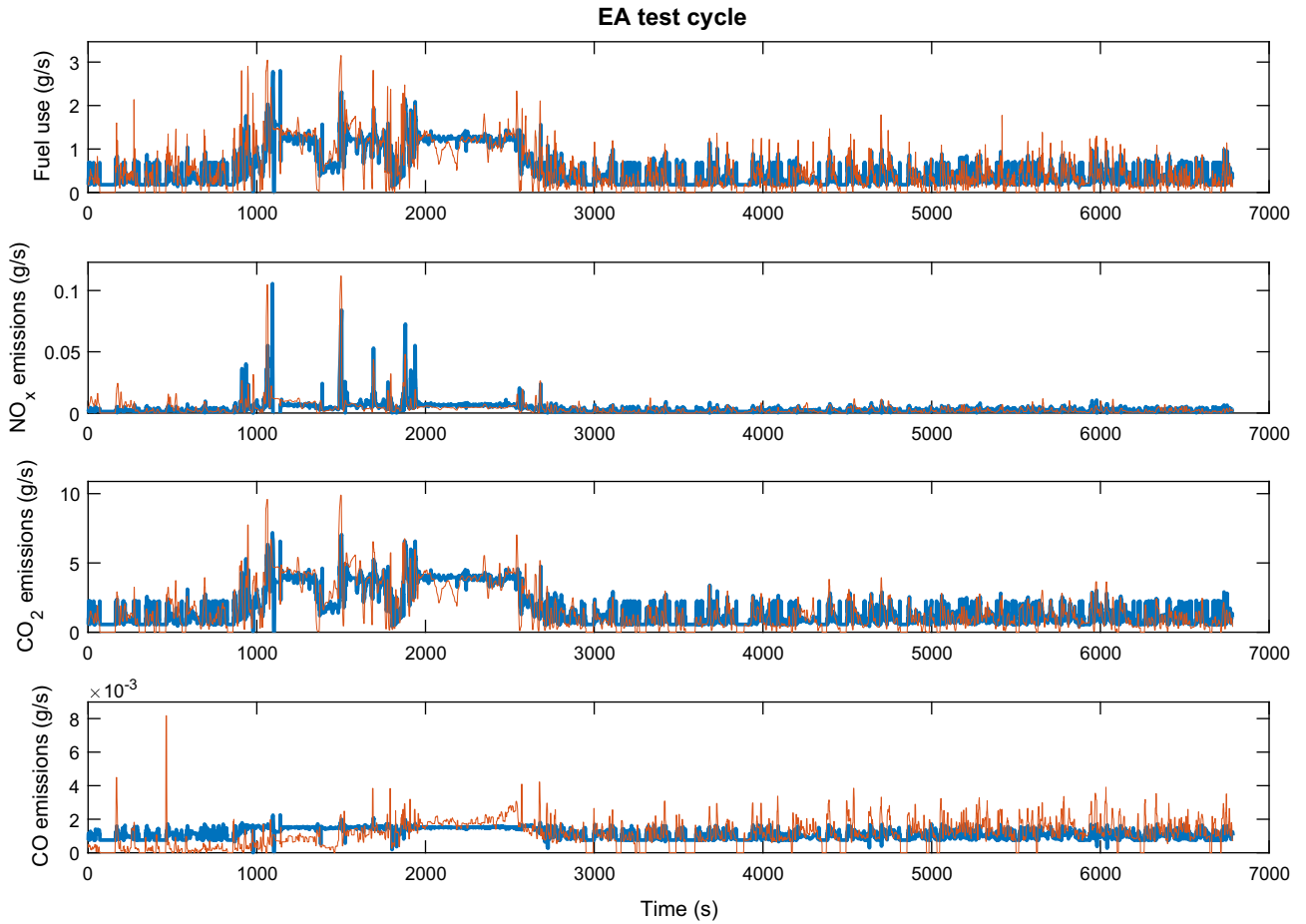


Fig. 13. Time series of observed (orange) and simulated (blue) mass of outputs using optimum bins for each output: (a) fuel use; (b) NO_x emissions; (c) CO₂ emissions; (d) CO emissions. (For interpretation of the references to color in this figure legend, the reader is referred to the web version of this article.)

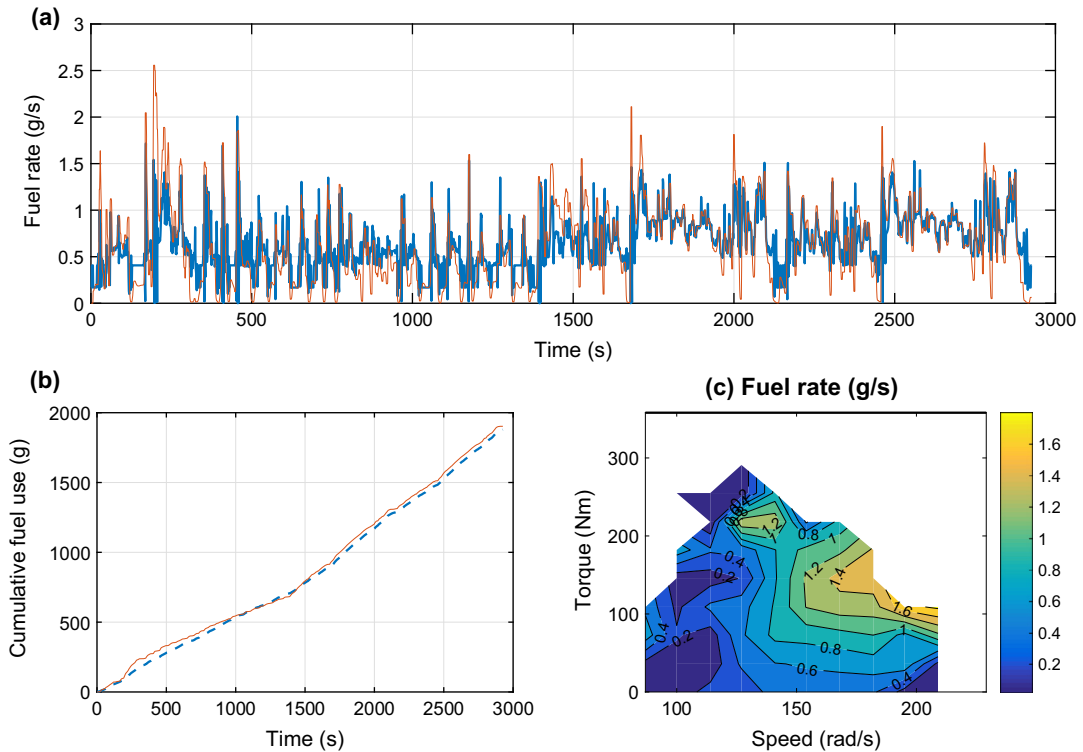


Fig. 14. (a) Observed (orange) and simulated (blue) fuel use over the ANL test cycle. (b) Cumulative sum of observed (orange) and simulated (blue) fuel use. (c) Engine map of transient fuel use created using the optimum bins for the ANL Chevrolet Cruze. The black lines represent the maximum torque envelope. (For interpretation of the references to color in this figure legend, the reader is referred to the web version of this article.)

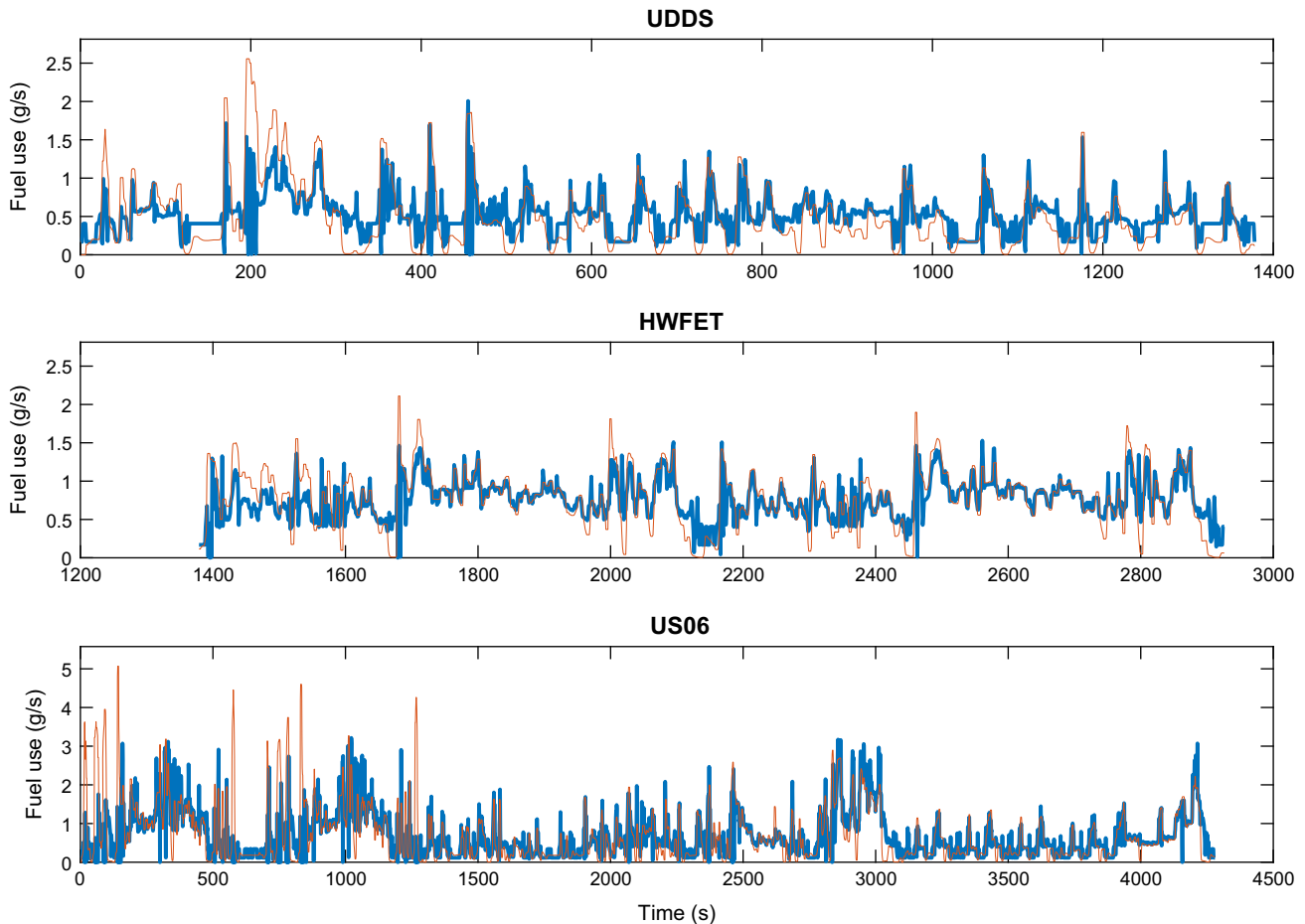


Fig. 15. Chevrolet Cruze observed (orange) and simulated (blue) fuel use using 10^2 bins over the (a) UDDS, (b) HWFET and (c) validated over the US06 driving cycle. (For interpretation of the references to color in this figure legend, the reader is referred to the web version of this article.)

function of shift speeds. The gearbox development is summarised in Fig. B.17.

The optimum vehicle configuration corresponded to an effective drag of 0.71 m^2 , a test mass of 1500 kg and rolling resistance coefficient of 0.0081 . As with the DAF CF 75, the method failed to replicate points at low engine speed and high torque. Optimum bins for each of the outputs were: 10^2 for fuel use and emissions of NO_x and CO_2 ; and 6^2 for CO emissions. Optimum vehicle configuration, observed and simulated engine torque, engine speed and wheel speed on a per second basis and the optimum bins for each output are illustrated in Fig. B.18. The optimum bins for each of the outputs were used to create the corresponding maps of instantaneous and brake specific outputs shown in Figs. 12 and B.20, respectively.

The EA route comprised motorway and non-motorway driving. Fig. 13 illustrates the accuracy of the method at reproducing the outputs on these two road types. Cumulative emissions of NO_x and CO_2 were 4.1% and 0.44% lower than the observed values, as seen in Fig. B.19 and reproduced per second driving accurately across both motorway and non-motorway driving. Cumulative fuel use and CO emissions were 0.26% and 1.7% higher than the observed values. However, there was a large discrepancy between simulated and observed CO emissions on a per second basis across the time series.

3.3. ANL Chevrolet Cruze

The Chevrolet Cruze had six gears. The development of its gearbox is summarised in Fig. B.21. The optimum vehicle configuration

corresponded to an effective drag of 0.64 m^2 , a test mass of 1731 kg and rolling resistance coefficient of 0.0081 . Optimum vehicle configuration, observed and simulated engine torque, engine speed and wheel speed on a per second basis and the optimum bins for fuel use are illustrated in Fig. B.22.

The optimum number of bins for fuel use was 10^2 with corresponding map shown in Fig. 14a. Here, the size of the white region illustrates the extent of the engine torque range which is not used in satisfying the per-second velocity of the training driving cycles. The equivalent brake specific fuel consumption map is given in Fig. 14c.

The method for the Chevrolet Cruze was developed on the UDDS and HWFET driving cycles, representing urban and highway driving, respectively. Fig. 15a and b illustrates the accuracy of the method at reproducing the outputs per driving type. The method reproduced well both the shape and magnitude of fuel use across both driving types. Cumulative fuel use was 1.3% lower than the observed value, as seen in Fig. 14b. The fuel use map was validated by simulating the Chevrolet Cruze over the US06 driving cycle which was a different data set from what the map was derived from. The magnitude and shape of simulated fuel use matches the observed values closely, as shown in Fig. 15c. At the trip level, simulated fuel use was 6.2% higher than the measured value.

ADVISOR and other powertrain simulation tools use hot and cold maps to predict accurately fuel use and emissions across a range of engine temperatures. Fuel use and emissions under cold running comprise a large proportion of the total for short trips. Consequently, regulatory limits of emissions, such as for NO_x and particle number, may be exceeded during both dynamometer

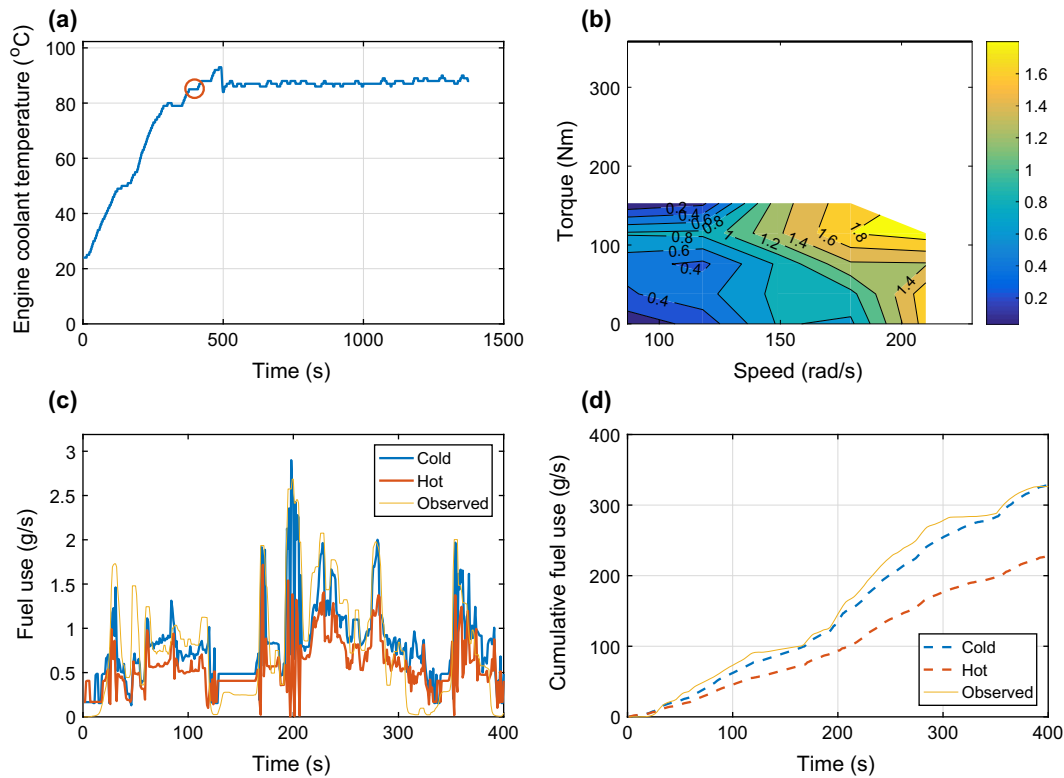


Fig. 16. (a) Plot of engine coolant temperature across the UDDS driving cycle with cold start. Orange circle indicates the transition from cold to hot running at 400 s. (b) Engine map of fuel use when running cold created using the optimum bins. Black line represents the maximum torque envelope. (c) Time series of fuel use when running cold using observed (yellow) data, simulated with cold map (blue) and simulated with original hot map (orange). (d) Cumulative sum of observed (yellow) and simulated fuel use using cold map (blue) and hot map (orange). (For interpretation of the references to color in this figure legend, the reader is referred to the web version of this article.)

[45] and on-road testing [25]. The influence of cold starts may be assessed also using physics-based models to capture the behaviour of the processes leading to increased fuel use and emissions [46].

The method in this paper was applied to a UDDS cold start at ambient (test cell temperature of 23 °C) using the earlier optimum vehicle configuration ($C_d A = 0.64 \text{ m}^2$, $C_{rr} = 0.0081$ and test mass = 1731 kg). New candidate maps were created based on the cold running fuel use. The engine was considered hot when the seven-second, one-dimensional median filter of engine coolant temperature stabilised and is shown in Fig. 16a. The index of transition from cold to hot emissions is indicated by the orange circle, corresponding to a engine coolant stabilisation temperature of 90 °C, which occurred after 400 s. The optimum number of bins was 5^2 for fuel use when running cold and the corresponding fuel use map is shown in Fig. 16b. Fig. 16d shows the observed fuel (yellow) use across the cold portion of the UDDS cold start cycle. Two simulated fuel uses are superposed: the blue time series shows fuel use using the cold map only; and in orange, fuel use using the hot maps created earlier. Simulated fuel use with the cold map underestimated observed cold running values by 0.6%. Fuel use was underestimated by 30% when the hot running map was used from the start.

Table A.2 contains the effective gear ratios and shift envelope positions for the three vehicles considered in this work. Table A.3 contains the optimum vehicle configurations, bin numbers for each output and corresponding sum of absolute deviations.

4. Conclusion

Poor urban air quality persists in global cities where large proportions of the population are exposed to harmful levels of pollutants. Regulations to address such emissions, including from road

vehicles, are becoming more strict. However, the gap is increasing between predicted (based on the regulatory tests) and real-world fuel use and emissions. One way to increase the accuracy of predictions is by using accurate engine maps simulated over real-world driving cycles.

This work presents a method to create engine maps using data gathered from OBD and PEMS while vehicles are operating in the real-world. This work is motivated by the ubiquity of OBD in modern vehicles and the requirement by new vehicle emissions regulations in Europe and the US to employ PEMS as part of in-use conformity tests. The regulatory push to use PEMS implies a large amount of real-world data will become available across a range of vehicles. This work is novel because it uses OBD and PEMS data directly. Conversely, existing methods require steady-state engine maps, obtained from a dynamometer test in most cases, to create a transient counterpart.

The method extracts the effective gear ratios from the OBD and uses PEMS output to create a large set of candidate engine maps. A sensitivity sweep of vehicle physical characteristics is used in ADVISOR to find the optimum vehicle configuration based on the smallest sum of Euclidean distances per second between the observed and simulated engine torque-speed pairs per configuration. Similarly, the optimum bins for fuel use and emissions correspond to the smallest sum of absolute deviations per second between observed and simulated data. The resulting maps reproduced accurately the shape and magnitude of fuel use and emissions for the three test vehicles presented such that the difference between simulated and observed cumulative fuel use and emissions was less than 5% in general.

The robustness of this method was demonstrated by applying it to both PEMS and vehicle dynamometer data, from a range of sources and across different vehicle types. This work is also fit

for a number of other purposes. For example, the method was applied to the UDDS cold start test to generate a cold fuel use engine map for the ANL Chevrolet Cruze. Additionally, the influence of emissions control technologies in the tailpipe of the DAF CF 75 was isolated by comparing maps of NO_x emissions at the output of the engine and at the tailpipe.

The availability of accurate engine maps across a range of vehicles can yield, including: insights into how control technologies can be tuned to reduce emissions under real-world driving by looking at hot spots in the maps; development of in-use emissions factors; identification of driving conditions corresponding to the most significant fuel use and emissions events; and accurate air quality modelling at the road segment level using simulated per second emissions from vehicles operating in the urban environment.

Acknowledgements

The authors acknowledge the UK EPSRC funding provided for this work under the Centre for Sustainable Road Freight Transport (EP/K00915X/1) and the Energy Efficient Cities Initiative (EP/F034350/1).

Appendix A. Supplementary material

Supplementary data associated with this article can be found, in the online version, at <http://dx.doi.org/10.1016/j.apenergy.2016.08.175>. Additional data related to this publication is available at the University of Cambridge data repository (<http://dx.doi.org/10.17863/CAM.1736>).

References

- [1] Edenhofer O et al., editors. *Climate change 2014: mitigation of climate change. Contribution of working group III to the fifth assessment report of the intergovernmental panel on climate change*. Cambridge University Press; 2014.
- [2] EEA. *Air quality in Europe – 2015 report*. European Environment Agency; 2015. Available from: <http://www.eea.europa.eu/publications/air-quality-in-europe-2015>.
- [3] EEA. *Annual European Union greenhouse gas inventory 1990–2014 and inventory report 2016*. European Environment Agency; 2016. Available from: <http://www.eea.europa.eu/publications/annual-european-union-greenhouse-gas/>.
- [4] Rexeis M et al. Update of emission factors for EURO 5 and EURO 6 vehicles for the HBEFA Version 3.2. Graz: Graz University of Technology; 2013. Available from: http://www.hbefa.net/e/documents/HBEFA32_EF_Euro_5_6_TUG.pdf [ch. Exhaust emissions from road transport].
- [5] USEPA. *Development of emission rates for light-duty vehicles in the motor vehicles emissions simulator (moves2010) Tech rep EPA-420-R-11-011*. Washington DC: Environmental Protection Agency; 2011. Available from: <http://www3.epa.gov/otaq/models/moves/documents/420r11011.pdf>.
- [6] Mock P et al. *From laboratory to road: a 2014 update of official and real-world fuel consumption and CO₂ values for passenger cars in Europe* White paper. Berlin: The International Council on Clean Transportation; 2014. Available from: http://www.theicct.org/sites/default/files/publications/ICCT_LaboratoryToRoad_2014_Report_English.pdf.
- [7] Franco V, Sánchez FP, German J, Mock P. Real-world exhaust emissions from modern diesel cars: a meta-analysis of PEMS emissions data from EU (Euro 6) and US (Tier 2 Bin 5/ULEV II) diesel passenger cars – Part 1: aggregated results White paper. Berlin: The International Council on Clean Transportation; 2014. Available from: http://www.theicct.org/sites/default/files/publications/ICCT_PEMS-study_diesel-cars_20141013.pdf.
- [8] USEPA. *Advanced light-duty powetrain and hybrid analysis (ALPHA) tool 2016*. Available from: <https://www3.epa.gov/otaq/climate/alpha.htm>.
- [9] ANL. *Autonomie 2016*. Available from: <http://www.autonomie.net/expertise/Autonomie.html>.
- [10] ACEA. *Reducing CO₂ emissions from heavy-duty vehicles*. European Automobile Manufacturers Association; 2016. Available from: https://www.acea.be/uploads/publications/ACEA_Position_Paper_Reducing_CO2_Emissions_from_Heavy-Duty_Vehicles.pdf.
- [11] Gao Z et al. A proposed methodology for estimating transient engine-out temperature and emissions from steady-state maps. *Int J Eng Res* 2010;11(2):137–51. <http://dx.doi.org/10.1243/14680874IER05609>.
- [12] Wu B et al. *Cam-phasing optimization using artificial neural networks as surrogate models – fuel consumption and NO_x emissions*. In: *SAE world congress, Detroit*.
- [13] Sayin C et al. Performance and exhaust emissions of a gasoline engine using artificial neural network. *Appl Therm Eng* 2007;27(1):46–54. <http://dx.doi.org/10.1016/j.applthermaleng.2006.05.016>.
- [14] Kiani MKD et al. Application of artificial neural networks for the prediction of performance and exhaust emissions in SI engine using ethanol-gasoline blends. *Energy* 2010;35(1):65–9. <http://dx.doi.org/10.1016/j.energy.2009.08.034>.
- [15] Ismail HM, Ng HK, Queck CW, Gan S. Artificial neural networks modelling of engine-out responses for a light-duty diesel engine fuelled with biodiesel blends. *Appl Energy* 2012;92:769–77. <http://dx.doi.org/10.1016/j.apenergy.2011.08.027>.
- [16] Roy S, Banerjee R, Bose PK. Performance and exhaust emissions prediction of a CRDI assisted single cylinder diesel engine coupled with EGR using artificial neural network. *Appl Energy* 2014;119:330–40. <http://dx.doi.org/10.1016/j.apenergy.2014.01.044>.
- [17] Çelik V, Arcaklioglu E. Performance maps of a diesel engine. *Appl Energy* 2005;81:247–59. <http://dx.doi.org/10.1016/j.apenergy.2004.08.003>.
- [18] Giakoumis EG, Alafouzou AI. Study of diesel engine performance and emissions during a transient cycle applying an engine mapping-based methodology. *Appl Energy* 2010;87(4):1358–65. <http://dx.doi.org/10.1016/j.apenergy.2009.09.003>.
- [19] Giakoumis EG, Lioutas SC. Diesel-engined vehicle nitric oxide and soot emissions during the European light-duty driving cycle using a transient mapping approach. *Transp Res Part D: Transp Environ* 2010;15(3):134–43. <http://dx.doi.org/10.1016/j.trd.2009.12.003>.
- [20] Frey HC, Zhang K, Roupail NM. Fuel use and emissions comparisons for alternative routes, time of day, road grade, and vehicles based on in-use measurements. *Environ Sci Technol* 2008;42(7):2483–9. <http://dx.doi.org/10.1021/es702493v>.
- [21] Yu L, Wang Z, Shi Q. *PEMS-based approach to developing and evaluating driving cycles for air quality assessment Tech rep 169300-1*. College Station: Southwest Region University Transportation Center; 2010.
- [22] Weiss M, Bonnel P, Hummel R, Provenza A, Manfredi U. On-road emissions of light-duty vehicles in Europe. *Environ Sci Technol* 2011;45(19):8575–81. <http://dx.doi.org/10.1021/es2008424>.
- [23] Kousoulidou M, Ntziachristos L, Gkeivanidis S, Samaras Z, Franco V, Dilara P. Validation of the COPERT road emission inventory model with real-use data. In: *19th International emission inventory conference, San Antonio*. Available from: <http://www.epa.gov/ttnchie1/conference/ei19/session6/dilara.pdf>.
- [24] Frey HC, Zhang K, Roupail NM. Vehicle-specific emissions modeling based upon on-road measurements. *Environ Sci Technol* 2010;44(9):3594–600. <http://dx.doi.org/10.1021/es902835h>.
- [25] May J, Bosteels D, Favre C. An assessment of emissions from light-duty vehicles using PEMS and chassis dynamometer testing. *SAE Int J Eng* 2014;7(3). <http://dx.doi.org/10.4271/2014-01-1581>.
- [26] Weiss M et al. Will Euro 6 reduce the NO_x emissions of new diesel cars? – Insights from on-road tests with portable emissions measurement systems (PEMS). *Atmos Environ* 2012;62:657–65. <http://dx.doi.org/10.1016/j.atmosenv.2012.08.056>.
- [27] Kousoulidou M, Fontaras G, Ntziachristos L, Bonnel P, Samaras Z, Dilara P. Use of portable emissions measurement system (PEMS) for the development and validation of passenger car emissions factors. *Atmos Environ* 2013;64:329–38. <http://dx.doi.org/10.1016/j.atmosenv.2012.09.062>.
- [28] EC. Commission Regulation (EU) No 582/2011 of 25 May 2011 implementing and amending Regulation (EC) No 595/2009 of the European Parliament and of the Council with respect to emissions from heavy duty vehicles (Euro VI) and amending Annexes I and III to Directive 2007/46/EC of the European Parliament and of the Council. *Off J Eur Union* 2011. Available from: <http://eur-lex.europa.eu/legal-content/EN/TXT/PDF/?uri=CELEX:32011R0582&from=EN>.
- [29] EPA. *Light-duty vehicle greenhouse gas emission standards and corporate average fuel economy standards*. Final rule EPA-420-F-10-014. Environmental Protection Agency; 2010. Available from: <http://www.epa.gov/oms/climate/regulations.htm#1-1>.
- [30] Weiss M, Bonnel P, Hummel R, Steinger N. A complementary emissions test for light-duty vehicles: assessing the technical feasibility of candidate procedures. Conclusions of the real-driving emissions – light-duty vehicles (RDE-LDV) working group. Joint Research Centre of the European Commission; 2013. Available from: http://publications.jrc.ec.europa.eu/repository/bitstream/JRC75998/ld-na-25572-en-n_online.pdf.
- [31] ANL. *Downloadable dynamometer database; 2016* [online].
- [32] Barlow TJ, Latham S, McCrae IS, Boulter PG. A reference book of driving cycles for use in the measurement of road vehicle emissions, no. PPR354. TRL Limited; 2009. Available from: http://www.gov.uk/government/uploads/system/uploads/attachment_data/file/4247/ppr-354.pdf.
- [33] USEPA. *Dynamometer drive schedules; 2016* [online].
- [34] DAF. *Specification sheet FT CF75 4x2 tractor; 2015* [online].
- [35] DAF. *PACCAR PR engines; 2016* [online].
- [36] ZF. *ZF technology in commercial vehicles: Automatic transmission; 2016* [online].
- [37] EC. *Directive 2005/55/EC of the European Parliament and of the Council of 28 September 2005 on the approximation of the laws of the Member States relating to the measures to be taken against the emission of gaseous and*

- particulate pollutants from compression-ignition engines for use in vehicles, and the emission of gaseous pollutants from positive-ignition engines fuelled with natural gas or liquefied petroleum gas for use in vehicles. Off J European Union 2005. Available from: <<http://eur-lex.europa.eu/legal-content/EN/TXT/PDF/?uri=CELEX:32005L0055&qid=1438266766754&from=EN>>.
- [38] Stenvall H. Driving resistance analysis of long haulage trucks at Volvo - test methods evaluation. Master's thesis in the Master's programme. Automotive Engineering; 2010. <<http://publications.lib.chalmers.se/records/fulltext/133658.pdf>>.
- [39] Parkers. Volkswagen Golf Hatchback (2009–2012) specs & dimensions; 2016 [online].
- [40] Jiménez JL et al. Vehicle specific power: a useful parameter for remote sensing and emission studies. In: 9th CRC on-road vehicle emissions workshop, San Diego. Available from: <http://cires1.colorado.edu/jjose/Papers/Jimenez_VSP_9thCRC_99_final.pdf>.
- [41] Fontaras G et al. Assessment of on-road emissions of four Euro V diesel and CNG waste collection trucks for supporting air-quality improvement initiatives in the city of Milan. *Sci Total Environ* 2012;426(1):65–72. <http://dx.doi.org/10.1016/j.scitotenv.2012.03.038>.
- [42] Parry IWH, Walls M, Harrington W. Automobile externalities and policies. RFF DP 06-26. Washington, DC: Resources for the Future; 2006. Available from: <<http://www.rff.org/rff/Documents/RFF-DP-06-26.pdf>>.
- [43] Pope III CA, Dockery DW. Health effects of fine particulate air pollution: lines that connect. *J Air Waste Manage Assoc* 2006;56(6):709–42. <http://dx.doi.org/10.1080/10473289.2006.10464485>.
- [44] WHO. Air quality guidelines - global update 2005. World Health Organization; 2006.
- [45] Favre C, Bosteels D, May J. Exhaust emissions from European market-available passenger cars evaluated on various drive cycles. In: 11th International conference on engines & vehicles, SAE. <http://dx.doi.org/10.4271/2013-24-0154>. Available from: <<http://www.aecc.be/content/pdf/SAE>>.
- [46] Weilenmann MF, Soltic P, Hausberger S. The cold start emissions of light-duty-vehicle fleets: a simplified physics-based model for the estimation of CO₂ and pollutants. *Sci Total Environ* 2013;444:161–76. <http://dx.doi.org/10.1016/j.scitotenv.2012.11.024>.